

# The Nuclear Structure and Associated Electron Capture Rates on Odd-Z Nucleus $^{51}\text{V}$ in Stellar Matter

Muneeb-Ur Rahman<sup>1</sup> • Jameel-Un Nabi<sup>2</sup>

**Abstract** The Gamow-Teller strength distribution function,  $B(\text{GT})$ , for the odd  $Z$  parent  $^{51}\text{V}$ ,  $N - Z = 5$ , up to 30 MeV of excitation energy in the daughter  $^{51}\text{Ti}$  is calculated in the domain of proton-neutron Quasiparticle Random Phase Approximation (pn-QRPA) theory. The pn-QRPA results are compared against other theoretical calculations, (n, p) and high resolution (d,  $^2\text{He}$ ) reaction experiments. For the case of (d,  $^2\text{He}$ ) reaction the calibration was performed for  $0 \leq E_j \leq 5.0$  MeV, where the authors stressed that within this excitation energy range the  $\Delta L = 0$  transition strength can be extracted with high accuracy for  $^{51}\text{V}$ . Within this energy range the current pn-QRPA total  $B(\text{GT})$  strength 0.75 is in good agreement with the (d,  $^2\text{He}$ ) experiment's total strength of  $0.9 \pm 0.1$ . The pn-QRPA calculated Gamow-Teller centroid at 4.20 MeV in daughter  $^{51}\text{Ti}$  is also in good agreement with high resolution (d,  $^2\text{He}$ ) experiment which placed the Gamow-Teller centroid at  $4.1 \pm 0.4$  MeV in daughter  $^{51}\text{Ti}$ . The low energy detailed Gamow-Teller structure and Gamow-Teller centroid play a sumptuous role in associated weak decay rates and consequently affect the stellar dynamics. The stellar weak rates are sensitive to the location and structure of these low-lying states in daughter  $^{51}\text{Ti}$ . The calculated electron capture rates on  $^{51}\text{V}$  in stellar matter are also in good agreement with the large scale shell model rates.

**Keywords** Gamow-Teller distribution; electron capture; pn-QRPA; stellar dynamics, supernovae

Muneeb-Ur Rahman

Department of Physics, Islamia College Peshawar, KPK, Pakistan

email: muneebtj@gmail.com

Jameel-Un Nabi

Faculty of Engineering Sciences, GIK Institute of Engineering Sciences and Technology, Topi 23640, Swabi, KPK, Pakistan

email: jameel@giki.edu.pk

## 1 Introduction

Supernovae are crucial to our very existence and for the dynamical/ morphological development of the universe. They are also at the nexus of many of the great debates raging among astronomers. These explosions have enriched the galaxy with oxygen we breathe, the iron in our blood, the calcium in our bones and teeth, and silicon which is used in the semiconductor-based electronic industries having enormous applications in this modern world. The weak interactions soften and smooth the landscape of star for gravity. These two forces play a pivotal role in cooking the material inside stellar kilns and play preeminent role in the make up of galaxies and stars formation and their physical death (supernova explosion). This is not only true for the star's energy budget but these forces help each other in a certain sense to change the composition of the stellar matter and entropy as well. When the ratio of neutrons to protons is low, electron capture is a more probable process to occur. The processes mediated by charge-changing weak interaction are 1) electron capture: 2) positron capture: 3)  $\beta^-$  decay in nucleus: 4)  $\beta^+$  decay. Gamow-Teller (GT) transitions play a preeminent role in the collapse of stellar core in the stages leading to a Type-II supernova. The GT strength distributions from ground and excited states are used for the calculation of weak decay rates for the core-collapse supernova dynamics and for probing the concomitant nucleosynthesis problem (1; 2; 3; 4; 5; 6).

The incarnation of the core-collapse mechanism is the conversion of a fraction of the gravitational energy into kinetic energy of the ejecta and internal energy of the inner core of the exploding star (7). The core collapse is the most energetic event in the universe with emitting energy budget of  $10^{46}$  J mostly in the form of neutrinos. When the temperature of the core becomes equal to or more than  $2.5 \times 10^9$  K, oxygen is set on fire

and silicon burning ensues when the inner core attains the temperature of  $3.5 \times 10^9$  K (8). At this instant the nucleosynthesis pushes the elements in the inner core to the iron group nuclei and when this inner core exceeds the appropriate Chandrasekhar mass limits it becomes unstable and inaugurates the implosion of the inner core and consequently announces the death of the star in an implosion and subsequent catastrophic explosion. The collapse of the star is very sensitive to the entropy and to the number of leptons per baryon,  $Y_e$  (2; 9). The neutrinos are considered as main sink of energy and lepton number until the core density reaches around  $10^{10} \text{gcm}^{-3}$ . At later stages of the collapse this assumption is no longer legitimate as electron capture rates increase with increase in stellar core density. This is primarily due to the reason that the Fermi energy of the electrons increases considerably as the stellar density increases by orders of magnitude. Example giving, for a fixed stellar temperature of  $3 \times 10^9$  K, the Fermi energy of the electrons is 0.00 MeV at a stellar density of  $10 \text{gcm}^{-3}$ . The Fermi energy increases to 0.00 MeV, 0.04 MeV, 2.36 MeV and 23.93 MeV as the stellar core stiffens to a density of  $10^3 \text{gcm}^{-3}$ ,  $10^5 \text{gcm}^{-3}$ ,  $10^8 \text{gcm}^{-3}$  and  $10^{11} \text{gcm}^{-3}$ , respectively. This increase in Fermi energy of electrons with increasing density makes the electrons more susceptible for getting captured and causes the electron capture rates to increase substantially. For densities greater than  $10^{11} \text{gcm}^{-3}$ , the neutrino mean free paths become shorter and consequently proceed through all phases of free streaming, diffusion, and trapping. The most tightly bound of all the nuclei in the inner core of star is  $^{56}\text{Fe}$  (10) and further fusion of the nuclei is endoergic. The second bottleneck to the synthesis of heavier elements is the high  $Z$  number which poses a high Coulombic barrier for the charged particles to initiate nuclear reactions at stellar core temperatures. These impediments to further nucleosynthesis is rescinded with the help of neutron (which do not feel the Coulomb barrier) capture processes in the stellar core to form heavier isotopes beyond iron group nuclei. These processes are further classified into slow (s-) and rapid (p-) neutron capture processes depending on the neutron capture time scale  $\tau_n$  and beta decay time scale  $\tau_\beta$  for nucleus to endure beta decay. As discussed earlier, weak interaction and gravity are the mentor that drives the stellar evolutionary process and its subsequent death in a cataclysmic explosion. The main weak interaction processes that play an effective role in the stellar evolution are beta decays, electron and positron capture processes and neutrinos emission/capture processes subject to the physical conditions available for these processes in the stellar core. These weak decay processes are smitten by Fermi and Gamow-Teller (GT)

transitions. Fermi transitions are straightforward and are important only for beta decays. Spin-isospin-flip excitations in nuclei at vanishing momentum transfer are commonly known as GT transitions. For nuclei with  $N > Z$ , Fermi transitions are Pauli blocked and the GT transitions dominate and their calculation is model dependent. These transitions are ideal probe to test nuclear structure and play preeminent role in the nucleosynthetic origin of the elements in the late phases of the stellar life. When the stellar matter is degenerate then the phase space for the electron in beta decay is Pauli blocked and electron captures become dominant in the stellar core producing neutrinos which escape from the surface of the star and takes away the core energy and entropy as well. These electron capture rates and  $\beta^+$  decay rates are very sensitive to the distribution of the  $\text{GT}_+$  strength (in this direction a proton is changed into a neutron).

$^{51}\text{V}$  plays a key role in the presupernova stages of evolution of massive stars, specially prior to the presupernova collapse of the stellar core (11).  $^{51}\text{V}$  is an important nucleus which is thought to play a significant role in neutrino-process productions and also thought to be a key gamma ray source (12). In this paper we present the Gamow-Teller strength distribution function in electron capture direction (referred to as  $\text{B}(\text{GT}_+)$  strength distribution) of  $^{51}\text{V}$  using the pn-QRPA model. The associated electron capture rates on  $^{51}\text{V}$  is also presented in stellar environment. We also compare and contrast our calculation with previous results.

Section 2 describes the theoretical formalism used for the  $\text{B}(\text{GT})$  strength and weak decay rates based on pn-QRPA model. Section 3 discusses the pn-QRPA calculated GT strength functions and its comparison with measurements and previous calculations. The calculated electron capture rates are presented in Sect. 4. We finally conclude our findings in Sect. 5.

## 2 Model Description

The pn-QRPA is considered an efficient model to extract the GT strengths for the ground as well as excited states of the nuclei present in stellar matter (13). The transitions from the excited states contribute effectively to the total electron capture rate and a microscopic calculation of excited state GT strength distributions is desirable. The pn-QRPA model is used in the present work to calculate the  $\text{B}(\text{GT}_+)$  strength distribution and associated electron capture rates on odd- $Z$  nucleus  $^{51}\text{V}$  using a luxurious model space of  $7\hbar\omega$ . The model is capable of performing a microscopic calculation of ground and excited states GT strength distribution functions.

The Hamiltonian used in our calculation is of the form

$$H^{\text{QRP}} = H^{\text{sp}} + V^{\text{pair}} + V_{\text{GT}}^{\text{ph}} + V_{\text{GT}}^{\text{pp}}, \quad (1)$$

where  $H^{\text{sp}}$  is the single-particle Hamiltonian,  $V^{\text{pair}}$  is the pairing force,  $V_{\text{GT}}^{\text{ph}}$  is the particle-hole (ph) GT force, and  $V_{\text{GT}}^{\text{pp}}$  is the particle-particle (pp) GT force. Pairing is treated in the *BCS* approximation, where an assumed constant pairing force with force strength  $G$  ( $G_p$  and  $G_n$  for protons and neutrons, respectively) is applied

$$V^{\text{pair}} = -G \sum_{jmj'm'} (-1)^{l+j-m} c_{jm}^+ c_{j-m}^+ (-1)^{l'+j'-m'} c_{j'm'} c_{j'-m'}, \quad (2)$$

here the sum over  $m$  and  $m'$  is restricted to  $m, m' > 0$ , and  $l$  donates the orbital angular momentum.

In the present work, in addition to the well known particle-hole GT force (14; 15; 16)

$$V_{\text{GT}}^{\text{ph}} = 2\chi \sum_{\mu} (-1)^{\mu} Y_{\mu} Y_{-\mu}^+, \quad (3)$$

with

$$Y_{\mu} = \sum_{j_p m_p j_n m_n} \langle j_p m_p | t_{-\sigma_{\mu}} | j_n m_n \rangle c_{j_p m_p}^+ c_{j_n m_n}, \quad (4)$$

the particle-particle GT force (17; 18)

$$V_{\text{GT}}^{\text{pp}} = -2\kappa \sum_{\mu} (-1)^{\mu} P_{\mu}^+ P_{-\mu}, \quad (5)$$

with

$$P_{\mu}^+ = \sum_{j_p m_p j_n m_n} \langle j_n m_n | (t_{-\sigma_{\mu}})^+ | j_p m_p \rangle (-1)^{l_n+j_n-m_n} c_{j_p m_p}^+ c_{j_n-m_n}^+, \quad (6)$$

is also taken into account.

The electron capture rate of a transition from the  $i$ th state of a parent nucleus ( $Z, N$ ) to the  $j$ th state of the daughter nucleus ( $Z-1, N+1$ ) is given by

$$\lambda_{ij}^{\text{ec}} = \ln 2 \frac{f_{ij}(T, \rho, E_f)}{(ft)_{ij}}. \quad (7)$$

In Eq. 7,  $f_{ij}$  is the phase space integral. The  $(ft)_{ij}$  of an ordinary  $\beta^{\pm}$  decay from the state  $|i\rangle$  of the mother nucleus to the state  $|f\rangle$  of the daughter is related to the reduced transition probability  $B_{ij}$  of the nuclear transition by

$$(ft)_{ij} = D/B_{ij}. \quad (8)$$

The  $D$  appearing in Eq. 8 is a compound expression of physical constants,

$$D = \frac{2\pi^3 \hbar^7 \ln 2}{g_V^2 m_e^5 c^4}, \quad (9)$$

whereas the reduced transition probability of the nuclear transition is given by

$$B_{ij} = B(F)_{ij} + (g_A/g_V)^2 B(GT)_{ij}. \quad (10)$$

The value of  $D$  is taken to be  $6146 \pm 6$  s adopted from Ref. (19) and the ratio of the axial-vector ( $g_A$ ) to the vector ( $g_V$ ) coupling constant is taken as -1.257.  $B(F)_{ij}$  and  $B(GT)_{ij}$  are reduced transition probabilities of the Fermi and GT transitions, respectively. These reduced transition probabilities of the nuclear transitions are given by

$$B(F)_{ij} = \frac{1}{2J_i + 1} | \langle j || \sum_k t_{\pm}^k || i \rangle |^2, \quad (11)$$

$$B(GT)_{ij} = \frac{1}{2J_i + 1} | \langle j || \sum_k t_{\pm}^k \vec{\sigma}^k || i \rangle |^2. \quad (12)$$

The phase space integrals are

$$f_{ij} = \int_{w_l}^{\infty} w \sqrt{w^2 - 1} (w_m + w)^2 F(+Z, w) G_- dw, \quad (13)$$

where  $G_-$  is the electron distribution function.  $F(+z, w)$  are the so-called Fermi functions and are calculated according to the procedure adopted by Ref. (20).  $w$  is the total energy of the electron including its rest mass,  $w_l$  is the total capture threshold energy (rest + kinetic) for electron capture.

The number density of electrons associated with protons and nuclei is  $\rho Y_e N_A$ , where  $\rho$  is the baryon density,  $Y_e$  is the ratio of electron number to the baryon number, and  $N_A$  is the Avogadro's number.

$$\rho Y_e = \frac{1}{\pi^2 N_A} \left( \frac{m_e c}{\hbar} \right)^3 \int_0^{\infty} (G_- - G_+) p^2 dp, \quad (14)$$

where  $p = (w^2 - 1)^{1/2}$  is the electron or positron momentum and  $G_+$  is the positron distribution function.

The total electron capture rate per unit time for a nucleus in thermal equilibrium at temperature  $T$  is then given by

$$\lambda_{\text{ec}} = \sum_{ij} P_i \lambda_{ij}^{\text{ec}}. \quad (15)$$

Here  $P_i$  is the probability of occupation of parent excited states and follows the normal Boltzmann distribution. The summation over all initial and final states is carried out until satisfactory convergence in the rate calculations is achieved.

### 3 Comparison of Gamow-Teller Strength Distributions for $^{51}\text{V}$

As discussed earlier  $^{51}\text{V}$  is a key nucleus which has a significant impact on the late stages of evolution of massive stars, specially prior to collapse (11). Potentially significant neutrino-process productions and gamma rays sources include many iron group nuclei including  $^{51}\text{V}$  (12). The GT strength distribution,  $B(\text{GT})$ , is calculated in the present work for the odd- $Z$  parent  $^{51}\text{V}$  up to 30 MeV of excitation energy in the daughter  $^{51}\text{Ti}$  using the pn-QRPA model. The distribution of the GT strength connecting the ground state of the parent  $^{51}\text{V}$  to the states in the daughter  $^{51}\text{Ti}$  in the  $\text{GT}_+$  direction is shown in Fig. 1 to Fig. 3. In Figs. 1 and 2 we compare our data with (d,  $^2\text{He}$ ) (21) and (n,p) reaction (22) experiments, respectively. The charge-exchange reactions near  $\theta = 0^\circ$  and at zero momentum transfer proceed fastidiously through Gamow-Teller transitions. The ground state of the parent is at  $J^\pi = 7/2^-$ , thereby allowing the GT transitions to the states in daughter with  $J^\pi = 5/2^-, 7/2^-$  and  $9/2^-$  (only allowed transitions are calculated in this work). Further we also compare our  $B(\text{GT}_+)$  strength distribution calculation with other theoretical calculations. In Fig. 1 to Fig. 3, the pn-QRPA strength is shown up to 12 MeV excitation for the sake of comparison only. The GT strength of the pn-QRPA is scaled with a quenching factor of 0.36. Aufderheide and collaborators (23) used larger model space in their shell model calculation and renormalized the calculated strength to the measured GT strength with a factor of 0.31 below 8 MeV.

We first compare our calculation with the (d,  $^2\text{He}$ ) reaction experiment. High-resolution studies of  $\text{GT}_+$  transitions are far more challenging to achieve as compared to studying high-resolution experiments of GT transitions in the  $\beta^-$  direction. When the two protons couple to an  $^1S_0, T = 1$  state, the unbound diproton system is referred to as  $^2\text{He}$ . Experimentally, the  $^1S_0$  is selected by limiting the relative energy of the diproton system to 1 MeV. The beam of 171 MeV deuterons was then targeted on the source (99.75 %  $^{51}\text{V}$  foils). The (d,  $^2\text{He}$ ) reaction experiments are complicated due to the coincident detection of the two correlated protons in the presence of an overwhelming background originating from deuteron breakup. However, since the reaction mechanism of (d,  $^2\text{He}$ ) forces a spin-flip, the reaction is more selective than the competing (n,p) and (t,  $^3\text{He}$ ) reactions. Further details of (d,  $^2\text{He}$ ) reaction experiment can be found in Ref. (21). Fig. 1 compares our  $B(\text{GT}_+)$  strength distribution calculation with the measured (d,  $^2\text{He}$ ) reaction carried out using the ESN-BBS setup of the superconducting cyclotron AGOR facility at KVI

Groningen (21). The calibration was performed for  $0 \leq E_j \leq 5.0$  MeV, and there the authors stressed that in this excitation energy range the transition strength can be extracted with high accuracy for  $^{51}\text{V}$ . Limiting the excitation energy to 5.0 MeV, the (d,  $^2\text{He}$ ) reaction gives total strength of  $0.9 \pm 0.1$ . The renormalized pn-QRPA total strength 0.79 for  $^{51}\text{V}$  is in good agreement with the measured strength of Ref. (21) for the same excitation energy range in daughter (additional GT strength at higher excitation energy above 5 MeV has not been included in this value). The pn-QRPA result for  $^{51}\text{V}$  is also compared with the blazing trails of pioneer calculation performed by Fuller, Fowler, and Newman (FFN) (24) in Fig. 1. FFN assumed that almost all the strength is concentrated in a collective state also referred to as GT resonance (GTR). FFN calculation placed the centroid of the GTR at 3.83 MeV of the excitation energy (also shown by a marked arrow in lower panel of Fig. 1). The pn-QRPA in present calculation yields GT centroid at 4.20 MeV in daughter  $^{51}\text{Ti}$ , and is in remarkable agreement with high resolution study of (d,  $^2\text{He}$ ) reaction data (21), which placed the centroid of the GT strength at  $4.1 \pm 0.4$  MeV.

On the other hand in (n,p) reaction experiments, a primary proton beam is first targeted on  $^7\text{Li}$ . Neutrons are then produced in the  $^7\text{Li}(p,n)$  reaction with the incoming proton beam of around 200 MeV energy. The resulting neutron beams are then targeted on the source (in the form of four foils of 99.5% pure vanadium targets of varying thickness). For further details of the (n,p) experiment we refer to (22) and references therein. Fig. 2 shows the comparison of pn-QRPA calculated  $B(\text{GT}_+)$  distribution with the measured  $^{51}\text{V}(\text{n}, \text{p})$  reaction at 198 MeV at TRIUMF (22). The spectroscopic information is available up to excitation energy 5.22 MeV for the daughter  $^{51}\text{Ti}$ , whereas in the pn-QRPA calculations discrete levels up to excitation energy of  $E_j = 8$  MeV are seen and beyond this very little strength is predicted. The (n,p) reaction (22) reports total strength of  $1.2 \pm 0.1$  up to 8 MeV for  $^{51}\text{V}$ . Aufderheide et al. (23) have analyzed the data for  $^{51}\text{V}$ , in the  $\text{GT}_+$  direction, up to excitation energy 12 MeV in daughter  $^{51}\text{Ti}$  and extracted total GT strength value of  $1.5 \pm 0.2$  for  $^{51}\text{V}$ . From pn-QRPA calculation, one finds little strength above 7 MeV of excitation energy when compared with the measured (n, p) data of Ref. (22) where reasonable strength is measured up to 10 MeV in daughter. We again show the placement of GTR centroid by FFN (24) by a marked arrow in the lower panel of Fig. 2. The dashed line at 6.33 MeV in lower panel of Fig. 2 indicates the maximum excitation energy considered in the (d,  $^2\text{He}$ ) reaction experiment (21), and defines the onset of the flat continuum response in the



spectrum. It will be interesting to snap whether high-lying GT strength exists above 6.33 MeV in the high resolution study of GT distribution, and such studies of the GT strength distribution can be done on the basis of angular distribution and a multipole decomposition (21).

The shell model calculation employing the KB3G interaction (25) using a quenching factor of 0.23 for  $^{51}\text{V}$  using the OXBASH code (26) in truncated model spaces is shown in Fig. 3. The shell model B(GT<sub>+</sub>) values were obtained adopting the Lanczos method with 100 iterations for each  $J^\pi$ . The shell model GT strength was normalized to the measured strength with a factor 0.74. The pn-QRPA calculated B(GT<sub>+</sub>) strength distribution seems to be in better accordance with the (d,  $^2\text{He}$ ) reaction data (21) and shell model calculation (25) as against the (n,p) reaction experiment (22). The shell model result placed the centroid of the calculated GT distribution at 4.34 MeV in daughter to be compared with 4.20 MeV calculated by this work. For sake of reference, the centroid of GTR calculated by FFN (24) is again shown by an arrow in the lower panel of Fig. 3. Marked also is the maximum excitation energy considered in the (d,  $^2\text{He}$ ) reaction experiment (21) as a dashed line at 6.33 MeV.

Caurier et al. (27) in their large-scale shell model calculation employed the monopole corrected version of the KB3 interaction and obtained a total GT strength of 1.4. This total strength is more in comparison to the reported pn-QRPA total strength and that measured in (d,  $^2\text{He}$ ) reaction experiment (21). The GT centroid in (27) is placed at a much higher energy of 5.18 MeV in daughter  $^{51}\text{Ti}$ . This centroid is around 1 MeV higher in energy than the centroid placements of pn-QRPA and high resolution (d,  $^2\text{He}$ ) data (21) and might suppress the weak decay rates of (27) in the stellar matter where the density and temperature is comparatively low.

#### 4 Electron Capture Rates

The stellar electron capture rates on  $^{51}\text{V}$  were calculated within the pn-QRPA formalism using the mass compilation of (28; 29) for temperature and density grid as summarized in Table 1, which additionally lists the chemical potential. The tabulated chemical potential refers to the electron kinetic energy and, thus shifted downward by the electron rest mass relative to the  $\mu_e$  values. The three selected temperature (density) points roughly depict low, medium and high temperature (density) zones.

The electron capture rates using the pn-QRPA in the present work are in excellent agreement with the large

scale shell model rates (30). The comparison of the two microscopic calculations is shown in Fig. 4. It is noted that the electron captures on  $^{51}\text{V}$  is quite sensitive to the temperature of the stellar core at low densities. At the first instant in low density regions the electrons have to overcome a threshold of nearly 3 MeV and this can be mainly achieved at low ( $\rho Y_e = 10^3 \text{gcm}^{-3}$ ) and intermediate densities ( $\rho Y_e = 10^7 \text{gcm}^{-3}$ ) by the thermal population of excited states in the parent  $^{51}\text{V}$ . The Fermi energies of the electrons, 0.046 MeV and 1.2 MeV, respectively, for these densities are still smaller than the Q-value of 2.47 MeV. The population index for the parent increases with temperature at these low density regime and consequently electron capture increases with the increase in temperature. As the stellar core approaches densities prior to presupernova epoch, the electron capture rates are no more dependent on the stellar temperature. At this stage the driving force for the electron captures is the chemical potential which grows much faster than the nuclear Q-value. Thus, at higher densities sufficient electrons are available with energies above the Q-value and leads to enhancement of electron capture rates. It can be seen from Fig. 4 that for low and medium density domain the shell model rates are in excellent comparison with the reported rates. Only in high density range does the shell model rate roughly double the corresponding pn-QRPA calculated electron capture rate.

Additionally Fig. 4 shows the comparison of pn-QRPA calculated electron capture rates on  $^{51}\text{V}$  with the calculation of FFN (24). For  $^{51}\text{V}$ , the pn-QRPA electron capture rates are in good agreement with FFN rates (24) at stellar core densities in the range  $\rho Y_e = 10^3 \text{gcm}^{-3}$  to  $10^7 \text{gcm}^{-3}$ . As the stellar core shifts to higher temperatures, the FFN rates get enhanced by a factor of two. The reasons for enhancement in the FFN rates could be attributed to at least two reasons. FFN, like the large scale shell model calculation, used Brink's hypothesis in their calculation (Brink's hypothesis states that GT strength distribution on excited states is *identical* to that from ground state, shifted *only* by the excitation energy of the state). FFN did not take into account the particle emission processes from higher excited states. As a result the parent excited states and resulting GT transitions (using Brink's hypothesis) extended beyond particle emission threshold energies. These states had a finite occupation probability at high temperatures and consequently significant contribution to total electron capture rates as can be seen from Eq. 15. Another reason for enhancement in the capture rates of FFN is due to the placement of GT centroid at too low energy in daughter nucleus (for details see (27; 31; 32)). In high density region the FFN

rates are bigger by roughly an order of magnitude for all temperature ranges for reasons already mentioned.

For modeling and simulation of a successful explosion mechanism one needs weak interaction mediated rates for chain of hundreds of nuclei as these weak rates are used as important nuclear physics input parameter in the simulation codes for core-collapse supernovae. Few of such important weak rates were presented earlier (e.g. (33; 34; 35; 36; 37; 38)). Work is still in progress for improved microscopic calculation of weak rates of remaining key iron-regime nuclei.

## 5 Summary

GT<sub>+</sub> transitions largely determine electron capture rates in the stellar core. Consequently GT strength is an important ingredient related to the complex dynamics of presupernova and supernova explosion. The GT<sub>+</sub> distribution for odd-Z <sup>51</sup>V nucleus has been calculated within the domain of pn-QRPA theory using a luxurious model space of  $7\hbar\omega$ . The comparison of the pn-QRPA model with high resolution (d,<sup>2</sup>He) experiment, with experimental results of (n, p), and with theoretical calculations of shell model and FFN has been made. The total GT strength and the GT centroid calculated within the domain of pn-QRPA is in good agreement with reported high resolution (d,<sup>2</sup>He) experimental value. The stellar weak decay rates are sensitive to the location of GT centroid and structure of these low-lying states in daughter <sup>51</sup>Ti. The small changes in the binding and excitation energies lead to significant modifications of the predictions for the synthesis of elements in the stellar kline. The good agreement of the low-lying pn-QRPA calculated GT strength with experimental results can affect the prediction and synthesis of <sup>51</sup>Ti as well as the time evolution and dynamics of the collapsing supermassive stars. FFN calculation placed the GT centroid of the GTR at 3.83 MeV excitation energy in daughter. The pn-QRPA calculation yields GT centroid at 4.20 MeV in daughter <sup>51</sup>Ti, and is in remarkable agreement with high resolution study of GT strength distribution (21), which placed centroid of the GT strength at  $4.1 \pm 0.4$  MeV. The shell model calculations placed it at 4.34 MeV. Within the energy range measurement of around 5 MeV, the current pn-QRPA total B(GT) strength 0.75 is also in good agreement with the (d, <sup>2</sup>He) experiment's total strength of  $0.9 \pm 0.1$ .

The calculated electron capture rates on <sup>51</sup>V in stellar matter are in excellent agreement with the large scale shell model rates for all temperature range. Only at high density of around  $\rho Y_e = 10^{11} \text{ g cm}^{-3}$  do the pn-QRPA rates get suppressed by a factor of two. The

corresponding comparison with FFN rates is fair and the pn-QRPA electron capture rates are suppressed by roughly an order of magnitude in high density region. Brachwitz et al. (39) performed model calculations for Type-Ia supernovae using FFN electron capture rates yielding overproduction of iron group nuclei. Type-Ia supernovae are responsible for about half of the abundances of the iron-group nuclei in the galactic evolution (40). It might be interesting for the simulators to study how the composition of the ejecta would be effected using the present smaller electron capture rates and to compare it with the observed abundances using supernovae simulation codes.

Realistically speaking weak interaction mediated rates of hundreds of nuclei are involved in the complex dynamics of supernova explosion. Incidentally, the most abundant nuclei tend to have small weak rates as they are more stable and the most reactive nuclei tend to be present in minor quantities. It is therefore the product of the weak rate and nuclear abundance of a particular specie which is more important in stellar core. We are in the process to calculate both the nuclear abundance and the weak decay rates for nuclei, which are considered to be important in astrophysical environment, as part of this on-going project.

## References

- Nabi, J.-U, Rahman, M.-U.-: Gamow-Teller transitions from  $^{24}\text{Mg}$  and their impact on the electron capture rates in the O+Ne+Mg cores of stars. *Phys. Rev. C* **75**, 035803 (2007).
- Nabi, J.-U, Rahman, M.-U: Gamow-Teller strength distributions and electron capture rates for  $^{55}\text{Co}$  and  $^{56}\text{Ni}$ . *Phys. Lett.* **B612**, 190-197 (2005).
- Fujita, Y., Adachi, T., Brentano, P. von Berg, G. P. A., Fransen, C., De Frenne, D., Fujita, H., Fujita, K., Hatanaka, K., Jacobs, E., Nakanishi, K., Negret, A., Pietralla, N., Popescu, L., Rubio, B., Sakemi, Y., Shimbara, Y., Shimizu, Y., Tameshige, Y., Tamii, A., Yosoi, M., Zell, K. O.: Gamow-Teller strengths in proton-rich exotic nuclei deduced in the combined analysis of mirror transitions. *Phys. Rev. Lett.* **95**, 212501 (2005).
- Nabi, J.-U, Rahman, M.-U: Gamow-Teller strength distribution in proton-rich nucleus  $^{57}\text{Zn}$  and its implications in astrophysics. *Astrophys Space Sci.* **332**, 309317 (2011).
- Zhi, Q., Langanke, K., Martinez-Pinedo, G., Nowacki, F., Sieja, K.: The  $^{76}\text{Se}$  Gamow-Teller strength distribution and its importance for stellar electron capture rates. *Nuclear Physics A* **859**, 172184 (2011).
- Sasano, M., Sakai, H., Yako, K., Wakasa, T., Dozono, M., Rodin, V., Faessler, A., Fujita, K., Greenfield, M. B., Hatanaka, K., Itoh, K., Kawabata, T., Kuboki, H., Maeda, Y., Miki, K., Muto, K., Noji, S., Okamura, H., Sakemi, Y., Sekiguchi, K., Shimizu, Y., Sasamoto, Y., Tameshige, Y., Tamii, A., Uesaka, T.: Gamow-Teller transition strengths in the intermediate nucleus of the  $^{116}\text{Cd}$  double- decay by the  $^{116}\text{Cd}(p, n)^{116}\text{In}$  and  $^{116}\text{Sn}(n, p)^{116}\text{In}$  reactions at 300 MeV. *Phys. Rev. C* **85**, 061301(R) (2012).
- Burrows, A., Livne, E., Dessart, L., Ott, C. D., Murphy, J.: Features of the acoustic mechanism of core-collapse supernova explosions. *Astrophys. J.* **640**, 878-890 (2006).
- Liu J-J, and Luo Z-Q: Effect of Strong Magnetic Field on GamowTeller Transition Electron Capture of Iron Group Nuclei at Crusts of Neutron Stars. *Commun. Theor. Phys.* (Beijing, China) **49**, 239-242 (2008).
- Bethe, H. A., Brown, G. E., Applegate, J., Lattimer, J. M.: Equation of state in the gravitational collapse of stars. *Nucl. Phys. A* **324**, 487 (1979).
- Cowan, J. J., Thielemann, F.-K.: R-process nucleosynthesis in supernovae. *Phys. Today*, **57**, 47 (2004).
- Bethe H.A., Brown G.E., Applegate J., Lattimer J.M.: Equation Of State In The Gravitational Collapse Of Stars. *Nucl. Phys. A* **324**, 487 (1979).
- Haxton, W. C.: Supernova Neutrino-Nucleus Physics and the r-process. Presented at 1st Argonne / MSU / JINA / INT RIA Workshop: The R-Process: The Astrophysical Origin Of The Heavy Elements And Related Rare Isotope Accelerator Physics. Edited by Qian Y-Z, Rehm E., Schatz H., Thielemann F.-K. 2004. (Proceedings from the Institute for Nuclear Theory, Vol. 13). Also as arXiv:nucl-th/0406012v1 4 Jun 2004.
- Nabi J.-U, Johnson C. W.: Comparison of Gamow-Teller strengths in the random phase approximation. *J. Phys. G* **40**, 065202 (2013).
- Halbleib, J. A., Sorensen, R. A.: Gamow-Teller beta decay in heavy spherical nuclei and the unlike particle-hole rpa. *Nucl. Phys. A* **98**, 542 (1967).
- Staudt, A., Hirsch, M., Muto, K., Klapdor-Kleingrothaus, H. V.: Calculation of -delayed fission of  $^{180}\text{Tl}$  and application of the quasiparticle random-phase approximation to the prediction of  $\beta^+$ -decay half-lives of neutron-deficient isotopes. *Phys. Rev. Lett.* **65**, 1543 (1990).
- Muto, K., Bender, E., Oda, T., Klapdor-Kleingrothaus, H. V.: Proton-neutron quasiparticle RPA with separable Gamow-Teller forces. *Z. Phys. A* **341**, 407 (1992).
- Soloviev, V. G.: Fragmentation of single-particle and collective motions in the quasiparticlephonon nuclear model. *Prog. Part. Nucl. Phys.* **19**, 107 (1987).
- Kuzmin, V. A., Soloviev, V. G.: Gamow-Teller  $\beta^+$  decays and strength functions of (n, p) transitions in spherical nuclei. *Nucl. Phys. A* **486**, 118 (1988).
- Jokinen, A., Nieminen, A., yst, J., Borcea, R., Caurier, E., Dendooven, P., Gierlik, M., Grska, M., Grawe, H., Hellstrm, M., Karny, M., Janas, Z., Kirchner, R., La Commar, M., Martínez-Pinedo, G., Mayet, P., Penttil, H., Plochocki, A., Rejmund, M., Roeckl, E., Sawicka, M., Schlegel, C., Schmidt, K., Schwengner, R.: Beta decay of  $^{57}\text{Zn}$ . *Euro. Phys. J. Direct A* **3**, 1 (2002).
- Gove, N. B., Martin, M. J.: Log-f tables for beta decay. *Nucl. Data Tables* **10**, 205 (1971).
- Bumer, C., Van den Berg, A. M., Davids, B., Frekers, D., De Frenne, D., Grewe, E.-W., Haefner, P., Harakeh, M. N., Hofmann, F., Hunyadi, M., Jacobs, E., Junk, B. C., Korff, A., Langanke, K., Martinez-Pinedo, G., Negret, A., von Neumann-Cosel, P., Popescu, L., Rakers, S., Richter, A., Wrtche, H. J.: High-resolution study of the Gamow-Teller strength distribution in  $^{51}\text{Ti}$  measured through  $^{51}\text{V}(d, ^2\text{He})^{51}\text{Ti}$ . *Phys. Rev. C* **68**, 031303(R) (2003).
- Alford, W. P., Brwon, B.A., Burzynski, S., Celler, A., Frekers, D., Helemer, R., Henderson, R., Jackson, K. P., Lee, K., Rahav, A., Trudel, A. Vetterli, M. C.: Spin-isospin strength distributions in f-p shell nuclei: A study of the  $^{51}\text{V}(n, p)$  and  $^{59}\text{Co}(n, p)$  reactions at 198 MeV. *Phys. Rev. C* **48**, 2818 (1993).
- Aufderheide, M. B., Bloom, S. D., Resler, D. A., Mathews, G. J.: Shell-model calculations of Gamow-Teller strength in  $^{51}\text{V}$ ,  $^{54}\text{Fe}$ , and  $^{59}\text{Co}$ . *Phys. Rev. C* **48**, 1677 (1993).
- Fuller, G. M., Fowler, W. A., Newman, M. J.: Stellar Weak interaction rates for intermediate mass nuclei. III. Rate tables for the free nucleons and nuclei with  $A = 21$  to  $A = 60$ . *Astrophys. J. Suppl. Ser.* **48**, 279 (1982).
- Poves, A., Snchez-Solano, A., Caurier, E., Nowacki, F.: Shell model study of the isobaric chains  $A = 50$ ,  $A = 51$  and  $A = 52$ . *Nucl. Phys. A* **694**, 157 (2001).
- Brown, B. A., Etchegoyen, A., Rae, W. D. M., Godwin, N. S.: Oxford-Buenos Aires-MSU shell model code (OXBASH), MSUCL Report No. 524, 1986.
- Caurier, E., Langanke, K., Martínez-Pinedo, G., Nowacki, F.: Shell-model calculations of stellar weak interaction rates. I. Gamow-Teller distributions and spectra of nuclei in the mass range  $A = 4565$ . *Nucl. Phys. A* **653**, 439(1999).
- Audi, G., Bersillon, O., Blachot, J., Wapstra, A. H.: The NUBASE evaluation of nuclear and decay properties. *Nucl. Phys. A* **729**, 3 (2003a).

- 
- Audi, G., Wapstra, A. H., Thibault, C.: The AME2003 atomic mass evaluation (II): tables, graphs and references. Nucl. Phys. **A729**, 337 (2003b).
- Langanke, K., Martínez-Pinedo, G.: Rate tables for the weak processes of pf-shell nuclei in stellar environments. ADNDT **79**, 1-46 (2001).
- Langanke, K., Martínez-Pinedo, G.: Supernova electron capture rates for Co-55 and Ni-56. Phys. Lett. **B436**, 19(1998).
- Langanke, K., Martínez-Pinedo, G.: Shell model calculations of stellar weak interaction rates: II. Weak rates for nuclei in the mass range  $A = 45-65$  in supernovae environment. Nucl. Phys. **A673**, 481(2000).
- Rahman, M.-U.: The Gamow-Teller strength distributions and associated weak decay rates in stellar matter. Ph.D. thesis, GIK Institute of Eng. Sciences & Tech. Pakistan (2007).
- Nabi,J.-U, Sajjad, M., Rahman,M.-U.: Electron Capture Rates on Titanium Isotopes in Stellar Matter. Acta Phys. Pol. B **38**, 3203 (2007).
- Nabi,J.-U, Sajjad, M.: Comparative study of Gamow-Teller strength distributions in the odd-odd nucleus  $^{50}\text{V}$  and its impact on electron capture rates in astrophysical environments. Phys. Rev. C **76**, 055803 (2007).
- Nabi, J.-U, Sajjad, M.: Neutrino energy loss rates and positron capture rates on  $^{55}\text{Co}$  for presupernova and supernova physics. Phys. Rev. C **77**, 055802 (2008).
- Nabi,J.-U, Sajjad, M.: Expanded Calculations of Proton-Neutron Quasiparticle Random Phase Approximation (pn-QRPA) Electron Capture Rates on  $^{55}\text{Co}$  for Presupernova and Supernova Physics. Cand. J. Phys. **86**, 819 (2008)
- Nabi,J.-U: Weak-Interaction-Mediated Rates on Iron Isotopes for Presupernova Evolution of Massive Stars. Eur. Phys. J. A **40**, 223 (2009).
- Brachwitz, F., Dean, D. J., Hix, W. R., Iwamoto, K., Langanke, K., Martínez-Pinedo, G., Nomoto, K., Strayer, M. R., Thielemann, F.-K. and Umeda,H.: The role of electron captures in Chandrasekhar-mass models for Type Ia supernovae. Astrophys. J. **536**, 934 (2000).
- Cowan J. J. and Thielemann, F.-K.: R-process nucleosynthesis in supernovae. Phys. Today , October issue, 47(2004).



---

**Table 1:** Temperature and density points for which  $^{51}\text{V}$  electron capture rates are calculated.

$T_9(K)$	$\rho Y_e(gcm^{-3})$	$\mu_e(MeV)$
1	3	0.046
3	3	0.000
10	3	0.000
1	7	1.200
3	7	1.021
10	7	0.196
1	11	23.933
3	11	23.925
10	11	23.832

---

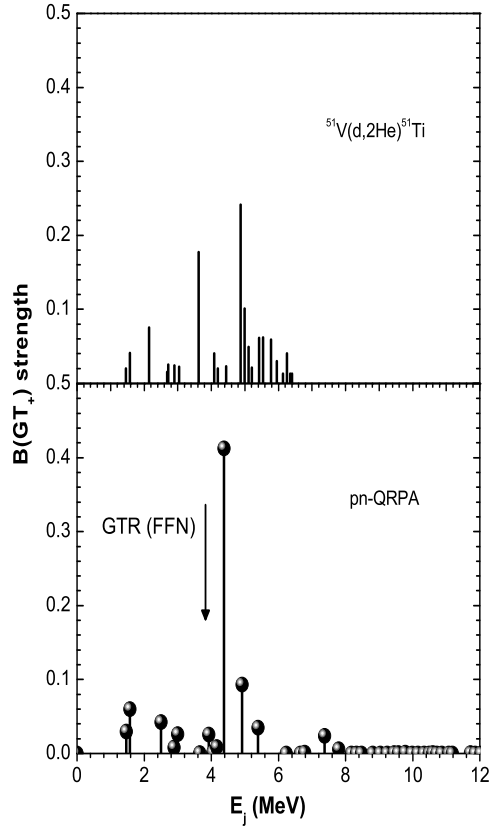


**Fig. 1** Comparison of the  $B(GT_+)$  strength distributions for  $^{51}\text{V}$  as function of excitation energy in  $^{51}\text{Ti}$  between pn-QRPA calculation (present work) and  $(d, ^2\text{He})$  reaction (21). The arrow denotes the position of the centroid of the GT resonance predicted by FFN (24).

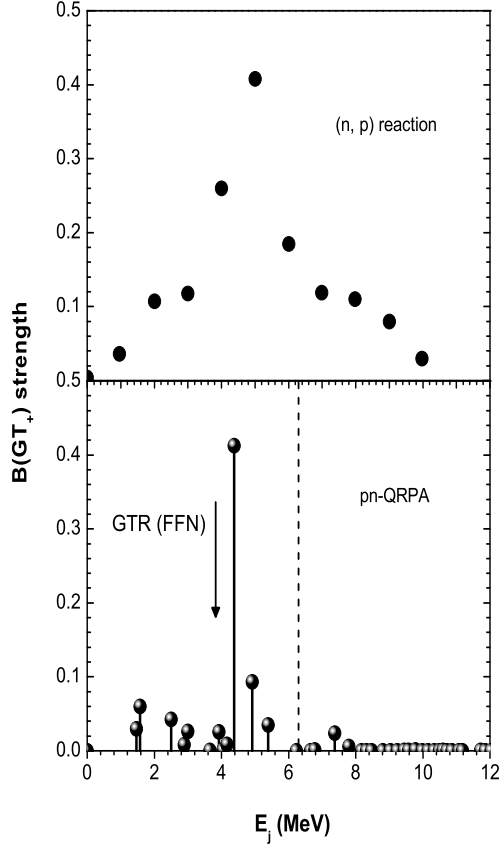


**Fig. 2** Comparison of the  $B(GT_+)$  strength distributions for  $^{51}\text{V}$  as function of excitation energy in  $^{51}\text{Ti}$  between pn-QRPA calculation (present work) and (n,p) experiment at TRIUMF (22). The arrow denotes the position of the centroid of the GT resonance predicted by FFN (24) and the dashed line represents the maximum energy considered in the (d,  $^2\text{He}$ ) reaction experiment (21).

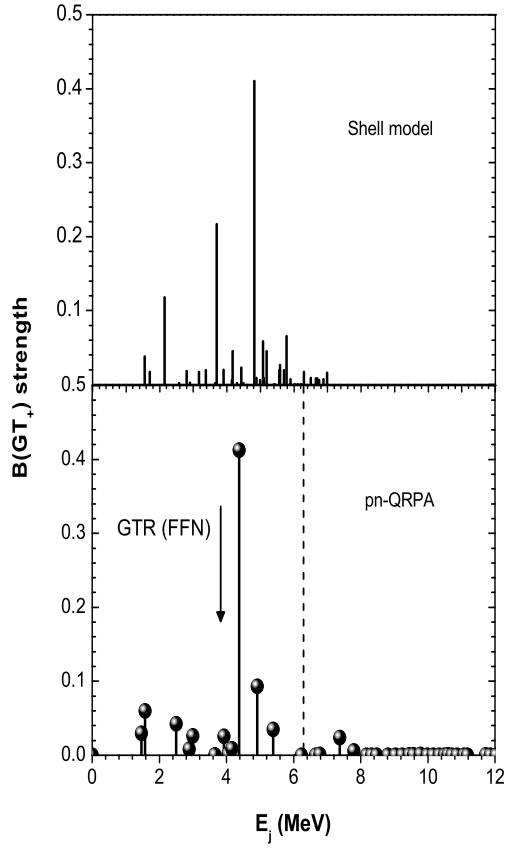


**Fig. 3** Comparison of the  $B(GT_+)$  strength distributions for  $^{51}\text{V}$  as function of excitation energy in  $^{51}\text{Ti}$  between pn-QRPA calculation (present work) and shell model (25) results. The arrow denotes the position of the centroid of the GT resonance predicted by FFN (24) and the dashed line represents the maximum energy considered in the  $(d, {}^2\text{He})$  reaction experiment (21).

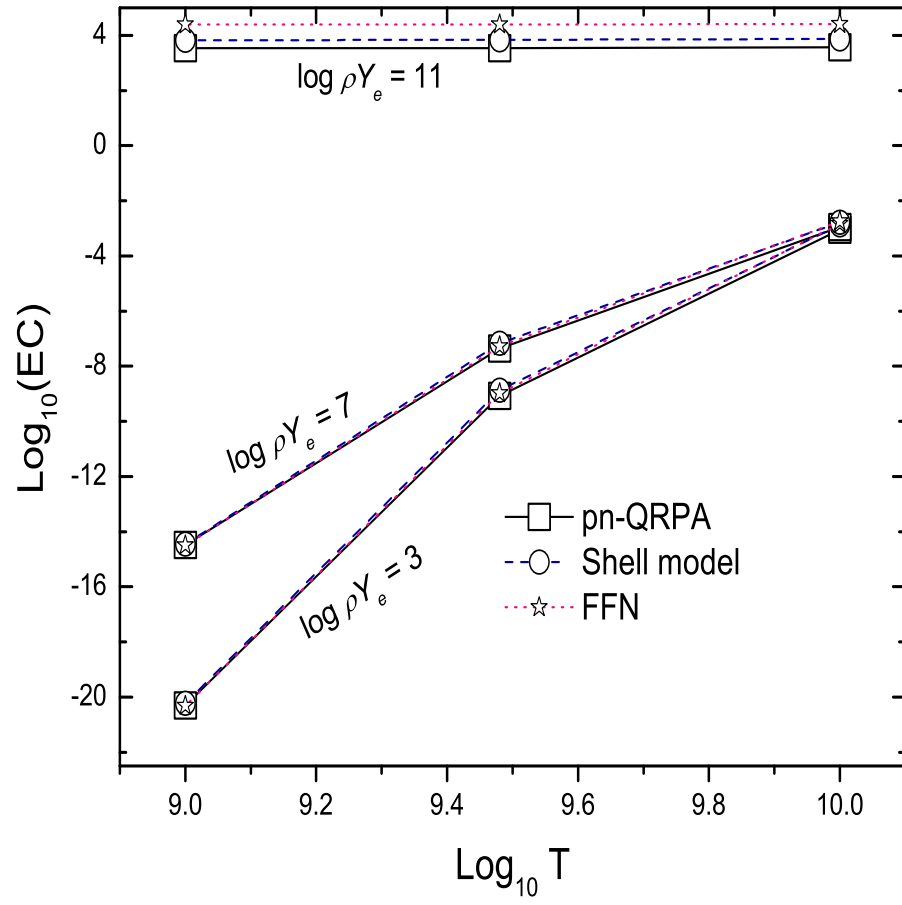


**Fig. 4** Comparison of the pn-QRPA, large scale shell model (30), and FFN (24) stellar electron capture rate calculations on  $^{51}\text{V}$  as a function of stellar temperature for selected densities.